TECHNICAL NOTES

NATIONAL ADVISORY COMMITTEE FOR AERONAUTICS

No. 544

AN APPLICATION OF THE VON KÁRMÁN-MILLIKAN LAMINAR BOUNDARY-LAYER THEORY AND COMPARISON WITH EXPERIMENT

By Albert E. von Doenhoff
Langley Memorial Aeronautical Laboratory

Washington
October 1935

NATIONAL ADVISORY COMMITTEE FOR AERONAUTICS

TECHNICAL NOTE NO. 544

AN APPLICATION OF THE VON KÁRMÁN-MILLIKAN LAMINAR BOUNDARY-LAYER THEORY AND COMPARISON WITH EXPERIMENT

By Albert E. von Doenhoff

SUMMARY

The von Kármán-Millikan theory of laminar boundary layers presented in N.A.C.A. Technical Report No. 504 is applied to the laminar boundary layer about an elliptic cylinder on which boundary-layer and pressure-distribution measurements were made at the National Bureau of Standards. An outline of the procedure of the von Kármán-Millikan method is given.

Good agreement is obtained between the calculated and experimental results, indicating that the method may be applied generally to the laminar boundary layer about any body provided that an experimentally determined pressure distribution is available. It appears that for all Reynolds Numbers above 24,000 the separation point for the elliptic cylinder should occur at a constant distance behind the point of minimum pressure, provided that the boundary layer does not become turbulent.

INTRODUCTION

From consideration of the relative order of magnitude of the various terms in the fundamental differential equations of flow, Prandtl has shown that the effects of viscosity at the high Reynolds Numbers common to aeronautical problems are of appreciable importance only in the thin fluid layer next to the surface of the body, thus considerably simplifying the fundamental equations. The actual solution of the boundary-layer equations has been a matter of considerable difficulty. It was shown, however, that separation of the flow from the surface is to be expected

when the boundary layer encounters rising pressures in the direction of flow.

The simplest case, that of the boundary layer along a flat plate with zero pressure gradient, has been successfully treated by Blasius. For this case no separation was to be expected. The treatment of the flow about bodies when pressure gradients exist has thus far not been completely successful. Numerous methods have been devised but either the prediction of the location of the separation point has been of doubtful accuracy or the methods have been applicable only to limited types of pressure distributions.

Experiments on an elliptic cylinder have been conducted at the National Bureau of Standards to study the separation phenomena and, in particular, to check the theory of Pohlhausen. (See reference 1.) The results, compared with Pohlhausen's approximate solution of the von Kármán integral equation, have demonstrated that the Pohlhausen method could only be depended upon to give reliable results when the pressure in the outside potential flow was decreasing; with increasing pressure separation may actually occur when Pohlhausen's method fails to indicate any flow separation.

Von Kármán and Millikan have recently devised a theory of laminar boundary layers involving separation (reference 2) that appears to have certain advantages over previous theories. This solution of the laminar boundary-layer problem can be applied more generally than former methods; the equation that is used to determine the separation point is a close approximation near the surface where the separation condition is applied, thus permitting a more accurate determination of the separation point.

The purpose of the present study is to investigate the extent to which the theory presented in reference 2 may be expected to give reliable results. This investigation was accomplished by applying the theory to the boundary layer about the elliptic cylinder on which the Bureau of Standards tests were made. A comparison is made between the calculated and experimental results, especially with reference to the location of the separation point.

EXPERIMENTAL DATA

The tests (reference 1) consisted of pressure-distribution and boundary-layer measurements on an elliptic cylinder. The pressure distribution was measured by a manometer connected to orifices in the surface of the cylinder. A hot-wire anemometer was used to make the boundary-layer surveys. The elliptic cylinder on which the tests were made had a major axis of 11.78 inches and a minor axis of 3.98 inches. It was placed in the air stream with the major axis parallel to the general flow. The tests were made at a Reynolds Number of approximately 24,000, based on the length of the minor axis.

OUTLINE OF THE VON KÁRMÁN-MILLIKAN PROCEDURE

The solution of the boundary-layer problem presented in reference 2 is divided into two parts, an outer and an inner solution. The outer solution is obtained by transforming the boundary-layer equation into a form analogous to that for the conduction of heat, the solution of which is well known. This part of the solution is most accurate in the region where the boundary-layer velocities are nearly equal to those in the outside stream, i.e., the outer part of the boundary layer. For reasons peculiar to the analysis, it is convenient to join the two solutions at an inflection point of the boundary-layer velocity profiles. Thus the range of this solution is taken as the region from the outer part of the boundary layer to the inflection point, or to the wall if no inflection point exists.

The inner solution is obtained by transforming the boundary-layer equation by certain approximations into an ordinary differential equation, which is most accurate near the wall. The inner solution is used only when the boundary-layer velocity profiles show an inflection point. Its range is then over the region from the wall to the inflection point.

The steps involved in computing the characteristics of the laminar boundary layer by this method follow.

Definition of dimensionless variables.- In the following computations the velocity at an infinite distance from the cylinder U_0 is considered to be the unit of ve-

locity. The minor axis l of the ellipse is used as the unit of length. These units of velocity and length lead to the formation of the following dimensionless quantities:

$R = \frac{U_o l}{\nu}$, Reynolds Number (ν, kinematic viscosity).

$\varphi^* = \frac{\varphi}{U_o l}$, nondimensional velocity potential.

$\psi^* = \frac{\psi}{U_o l} \frac{\sqrt{R}}{2}$, nondimensional stream function.

$u^* = \frac{u}{U_o}$, nondimensional velocity in the boundary layer.

$U^* = \frac{U}{U_o}$, nondimensional velocity just outside the boundary layer.

$z^* = \frac{\frac{U^2 - u^2}{2}}{U_o^2} = \frac{z}{U_o^2}$, nondimensional "energy defect" in the boundary layer.

In the following computations, the asterisks are dropped for simplicity, and nondimensional quantities thus formed are always to be understood.

Calculation of outer solution.- In order to calculate the outer solution, it is necessary to know the variation of the square of the outside velocity U^2 with the velocity potential φ along the surface. Reference 1 gives experimentally determined values of U as a function of the nondimensional distance s along the surface. This relation is plotted in figure 1. The velocity potential $\varphi = \int_0^s U ds$ is determined by a graphical integration of this curve. Both U and φ are then known as functions of the distance along the surface. The U^2, φ curve, shown in figure 2, is determined by choosing corresponding values of U and φ at several points along the surface.

The next step in the calculation is the expression of the U^2, φ curve in terms of power series. The calculations are greatly simplified if the U^2, φ curve is arbi-

trarily divided into two regions and a separate power series is used to approximate the curve in each region; that is, for

$$\varphi \leqq \varphi_1 \qquad U^2 = \sum_{i=0}^{n} b_i \varphi^i$$

$$\varphi \geqq \varphi_1 \qquad U^2 = \sum_{i=0}^{m} \beta_i \varphi^i$$

where φ_1 is the arbitrarily chosen value of φ separating the two regions. It was found possible in this investigation to obtain a satisfactory approximation to the experimental U^2,φ curve by using terms involving only up to the second power of φ. It appears that the U^2,φ curve should be fitted with greater care in the neighborhood of the separation point than elsewhere. The value of φ_1 chosen was 0.4. The following approximate expressions for the U^2,φ curve were then obtained:

for $\varphi \leqq 0.4$ $\qquad U^2 = 7.380\varphi - 8.855\varphi^2$

for $\varphi \geqq 0.4$ $\qquad U^2 = 1.393 + 0.414\varphi - 0.148\varphi^2$

The approximate U^2,φ curve, given by the foregoing expressions, is also shown in figure 2.

It is now possible to compute the energy defect z_ω, at any point in the boundary layer as a function of φ and ψ. (The subscript ω denotes the outer solution.)

$$z_\omega(\varphi,\psi) = \left\{\beta_0 h_0^* + \gamma_1\varphi_1 g_1^* - \gamma_2 \varphi_1^2 g_2^*\right\} + \varphi\left\{b_1(h_1 - h_1^*) + \beta_1 h_1^* + 2\gamma_2\varphi_1(g_1^* + g_2^*)\right\} + \varphi^2\left\{b_2(h_2 - h_2^*) + \beta_2 h_2^*\right\} \qquad (1)$$

for $\varphi \geqq \varphi_1$

$$\gamma_1 = b_1 - \beta_1 \qquad \gamma_2 = b_2 - \beta_2$$

For $\varphi \leqq \varphi_1$ put β_1, β_2, h_0^*, h_1^*, h_2^*, g_1^*, g_2^* equal to zero. The factors h_0, h_1, h_2, g_1, and g_2 are functions of $\frac{\psi}{\sqrt{\varphi}}$ only, and thus do not depend on

the particular case. The same functions as the foregoing but formed for the variable $\frac{\psi}{\sqrt{\varphi - \varphi_1}}$ are h_0^*, h_1^*, h_2^*, g_1^*, and g_2^*. Equation (1) corresponds to equation (19) in reference 2. The terms arising from the use of powers of φ greater than 2 have been deleted.

Substituting the values of the known coefficients in the expression for z_ω (equation (1)),

$$z_\omega = \left\{1.3930\ h_0^* + 2.7864\ g_1^* + 1.3931\ g_2^*\right\} + \varphi\left\{7.3800\ h_1 - 6.9660\ h_1^* - 6.9656\ g_1^* - 6.9656\ g_2^*\right\} + \varphi^2\left\{-8.8550\ h_2 + 8.7070\ h_2^*\right\} \qquad (2)$$

The functions g_0, g_1, g_2, h_0, h_1, h_2, are computed from the following relations:

$$g_0(\xi) = \frac{1}{2}\left(1 - P(\xi)\right), \qquad \xi = \frac{\psi}{\sqrt{\varphi}}$$

where $P(\xi)$ is the probability integral,

$$\frac{2}{\sqrt{\pi}} \int_0^\xi e^{-\beta^2}\, d\beta, \text{ a tabulated function.}$$

$$g_1(\xi) = -\frac{1}{\sqrt{\pi}}\,\xi\, e^{-\xi^2} + \xi^2\left(1 - P(\xi)\right)$$

$$g_2(\xi) = \frac{\xi\, e^{-\xi^2}}{3\sqrt{\pi}} - \frac{2}{3\sqrt{\pi}}\,\xi^3\, e^{-\xi^2} + \frac{2}{3}\,\xi^4\left(1 - P(\xi)\right)$$

$$h_0(\xi) = g_0(\xi)$$

$$h_1(\xi) = g_0(\xi) + g_1(\xi)$$

$$h_2(\xi) = g_0(\xi) + 2g_1(\xi) + g_2(\xi)$$

These functions are plotted throughout their useful range in figures 3 and 4.

In the subsequent calculations, the power-series expansions of these functions are required.

$$\left.\begin{aligned} g_0(\xi) &= 0.5000 - 0.5642\xi + 0.1881\xi^2 - 0.0564\xi^5 \\ g_1(\xi) &= -0.5642\xi + \xi^2 - 0.5642\xi^3 + 0.0940\xi^5 \\ g_2(\xi) &= 0.1881\xi - 0.5642\xi^3 + 0.6667\xi^4 - 0.2821\xi^5 \\ h_1(\xi) &= 0.5000 - 1.1284\xi + \xi^2 - 0.3761\xi^3 + 0.0377\xi^5 \\ h_2(\xi) &= 0.5000 - 1.5045\xi + 2\xi^2 - 1.5045\xi^3 + 0.6667\xi^4 - 0.1505\xi^5 \end{aligned}\right\} \quad (3)$$

It is now possible to compute the z_ω, ψ curves. This computation is performed by choosing the value of φ corresponding to the desired distance along the surface and calculating z_ω for several values of ψ by equation (2). The outer limit of the boundary layer is chosen as the point at which relative energy deficiency $\frac{z}{z_0} = 0.01$ where $z_0 = \frac{U^2}{2}$. The velocity is then 0.995 the outside velocity.

From the z_ω, ψ curves and the relations

$$u = U\sqrt{1 - \frac{z}{z_0}}$$

$$y\sqrt{R} = \frac{2}{U}\int_0^{\psi} \frac{d\psi}{\sqrt{1 - \frac{z}{z_0}}}$$

the velocity profiles in the boundary layer are obtained. Because the integrand in the expression for $y\sqrt{R}$ becomes infinite as the lower limit of integration is approached, it is necessary to evaluate the integral by a combination of graphic and analytic methods (reference 2, p. 10). For values of z near z_0, that is, for small values of ψ, z is expanded in a power series in ψ, using equations (2) and (3), and integrated analytically from $\psi = 0$ to some small value of ψ, say $\psi = 0.05$. From that point, the integration may be performed graphically by means of a planimeter or Coradi integraph.

In cases where the u,y (or z,ψ) curves have no inflection point, this procedure completes the solution for the particular value of φ chosen. When the u,y

curves have an inflection point, it is necessary to determine certain quantities from the outer solution at the inflection point to aid in fixing the boundary conditions for the inner solution.

The power series in ψ for z_ω is again used to determine the position of the inflection point. Since the inflection point, in general, occurs at small values of ψ, powers of ψ higher than ψ^3 may be neglected. The position of the inflection point is found by equating $\frac{\partial^2 z}{\partial \psi^2} = 0$, and solving for ψ. This value of ψ is denoted by $\psi_{\omega j}$ where the subscript j designates a joining-point characteristic. The values of $\left(\frac{\partial z}{\partial \xi}\right)_{\omega j}$ and z_j are then found by substituting $\psi_{\omega j}$ in the power-series expansions for these quantities. This procedure completes the outer solution when the boundary-layer velocity profiles have an inflection point.

Inner solution.- The inner solution is given (reference 2, equation (29)) in the form

$$\xi_i = \frac{1}{\sqrt{2}} \sqrt{\frac{z_o}{-z_o'\varphi}} \left(\frac{\zeta_j}{z_o}\right)^{3/4} \left[B - \sqrt{B^2 + 2\sqrt{\frac{\zeta_i}{\zeta_j}} - \frac{\zeta_i}{\zeta_j}} + \sin^{-1} \frac{1}{\sqrt{1 + B^2}} - \sin^{-1} \frac{1 - \sqrt{\frac{\zeta_i}{\zeta_j}}}{\sqrt{1 + B^2}} \right] \tag{4}$$

where $z_o' = \frac{\partial z_o}{\partial \varphi}$

$$\zeta = z_o - z = \frac{u^2}{2}$$

The subscript i denotes the inner solution; B is a constant of integration proportional to $\left(\frac{\partial u}{\partial y}\right)^2_{y=o}$; and z_o, z_o', and φ are derived directly from the outside pressure distribution, which has been experimentally determined. The value of ζ_j is taken from the outer solution and is equal to $z_o - z_{\omega j}$.

It is to be noted that $\frac{\partial^2 \zeta_i}{\partial \xi^2} = 0$ when $\zeta_i = \zeta_j$. Another boundary condition is that $\left(\frac{\partial \zeta_i}{\partial \xi}\right)_j = \left(\frac{\partial \zeta_\omega}{\partial \xi}\right)_j$. This condition gives the equation

$$\left(\partial \frac{\frac{\zeta_i}{z_o}}{\partial \xi}\right)_j = 2\sqrt{2}\sqrt{\frac{-z_o'\varphi}{z_o}}\left(\frac{\zeta_j}{z_o}\right)^{1/4}\sqrt{1+B^2} \qquad (5)$$

for determining B, the left-hand side of which is known from the outer solution. The value of B thus found is substituted in (4) and ξ_i is then computed for several values of the ratio $\frac{\zeta_i}{\zeta_j}$ between 0 and 1.

It will be found, in general, that ξ_{ij} is not equal to $\xi_{\omega j}$. In order to make the final solution continuous, the values of ξ_ω are shifted by an amount $\epsilon = \xi_{ij} - \xi_{\omega j}$, that is, for the outer solution $\xi = \xi_\omega + \epsilon$.

With this information, the ζ, ψ curve can be drawn continuously for both solutions. As before, the u,y profile is determined from this curve by the following relations

$$u = U\sqrt{\frac{\zeta}{z_o}}$$

$$y\sqrt{R} = \frac{2}{U}\int_0^{\psi} \frac{d\psi}{\sqrt{\frac{\zeta}{z_o}}}$$

For the inner solution, this integral may be expressed analytically. In this case

$$y\sqrt{R} = \frac{2\sqrt{\varphi}}{U} I_\xi$$

where

$$I_\xi = \frac{1}{\sqrt{2}}\sqrt{\frac{z_o}{-z_o'\varphi}}\left(\frac{\zeta_j}{z_o}\right)^{1/4}\left[\sin^{-1}\frac{1}{\sqrt{1+B^2}} - \sin^{-1}\frac{1-\sqrt{\frac{\zeta_i}{\zeta_j}}}{\sqrt{1+B^2}}\right]$$

Past the joining point, the integration is most easily carried out graphically.

Since B is proportional to $\left(\frac{\partial u}{\partial y}\right)^2_{y=0}$, the condition

for separation is that B shall equal zero. The position along the surface for which this relation holds is determined by trial and error.

RESULTS AND DISCUSSION

A comparison of the calculated velocity profiles and experimental results at several points along the surface of the elliptic cylinder is given in figures 5, 6, and 7. The calculated Pohlhausen curves, which have been discussed in reference 1, are shown for convenient comparison. The agreement becomes better forward of the separation point. Close to the separation point the calculations show, in general, too low velocities at corresponding distances from the surface, but the shape of the calculated separation point profile is in good agreement with the observed velocity distribution at the experimentally determined separation point.

The positions of the calculated and experimental separation points are indicated on the pressure-distribution diagrams shown in figure 8. The calculated separation point was found to occur at a distance along the surface $s = 1.92$. Actual separation was observed at $s = 1.99$. In view of the many approximations and arbitrary procedures involved in the analysis, this agreement is considered very good.

It is to be noted that the curves given in figures 5, 6, and 7 are independent of the Reynolds Number, except insofar as Reynolds Number affects the pressure distribution. It is, of course, assumed that the boundary layer does not become turbulent. An example of the effect of a change in the pressure distribution on the position of the separation point is given in figure 8, where the calculated separation point is shown for the perfect-fluid pressure distribution about the cylinder. In this case the position of the separation point is at $s = 2.38$, considerably aft the position found with the experimental pressure distribution. Figure 8 shows that, for both pressure distributions, the separation point occurs at approximately the same distance, $s = 0.7$, aft the point of minimum pressure. Since it is to be expected that the pressure distributions for higher Reynolds Numbers will be between the experimental curve shown and the perfect fluid-pressure distribution, this result indicates that for all Reynolds Num-

bers above 24,000 the separation point for the elliptic cylinder will occur at a distance $s = 0.7$, aft the point of minimum pressure provided, of course, that the boundary layer does not become turbulent.

A general view of the flow about the elliptic cylinder in the N.A.C.A. smoke tunnel is shown in figure 9. The effect of separation on the entire flow configuration should be noted.

CONCLUSIONS

The computed and experimental characteristics of the laminar boundary layer about the elliptic cylinder are in good agreement. This agreement indicates that the method may be generally applied to the laminar boundary layer about any type of body provided that an experimentally determined pressure distribution is available. It appears that for all Reynolds Numbers above 24,000 the separation point for the elliptic cylinder should occur at a constant distance behind the point of minimum pressure, provided that the boundary layer does not become turbulent.

Langley Memorial Aeronautical Laboratory,
National Advisory Committee for Aeronautics,
Langley Field, Va., October 10, 1935.

REFERENCES

1. Schubauer, G. B.: Air Flow in a Separating Laminar Boundary Layer. T.R. No. 527, N.A.C.A., 1935.

2. von Kármán, Th., and Millikan, C. B.: On the Theory of Laminar Boundary Layers Involving Separation. T.R. No. 504, N.A.C.A., 1934.

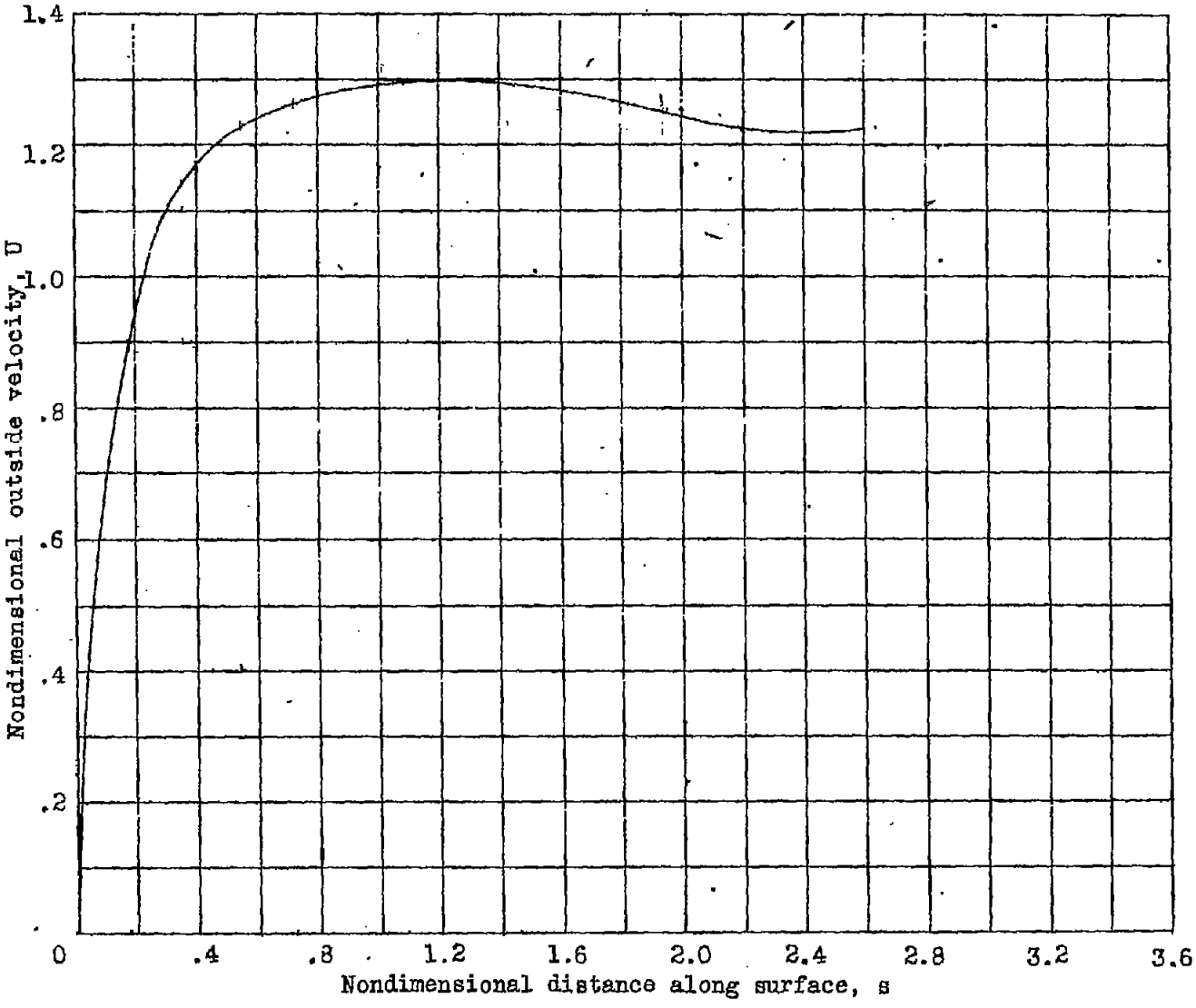

Figure 1.- Experimental velocity distribution along the surface of an elliptic cylinder.

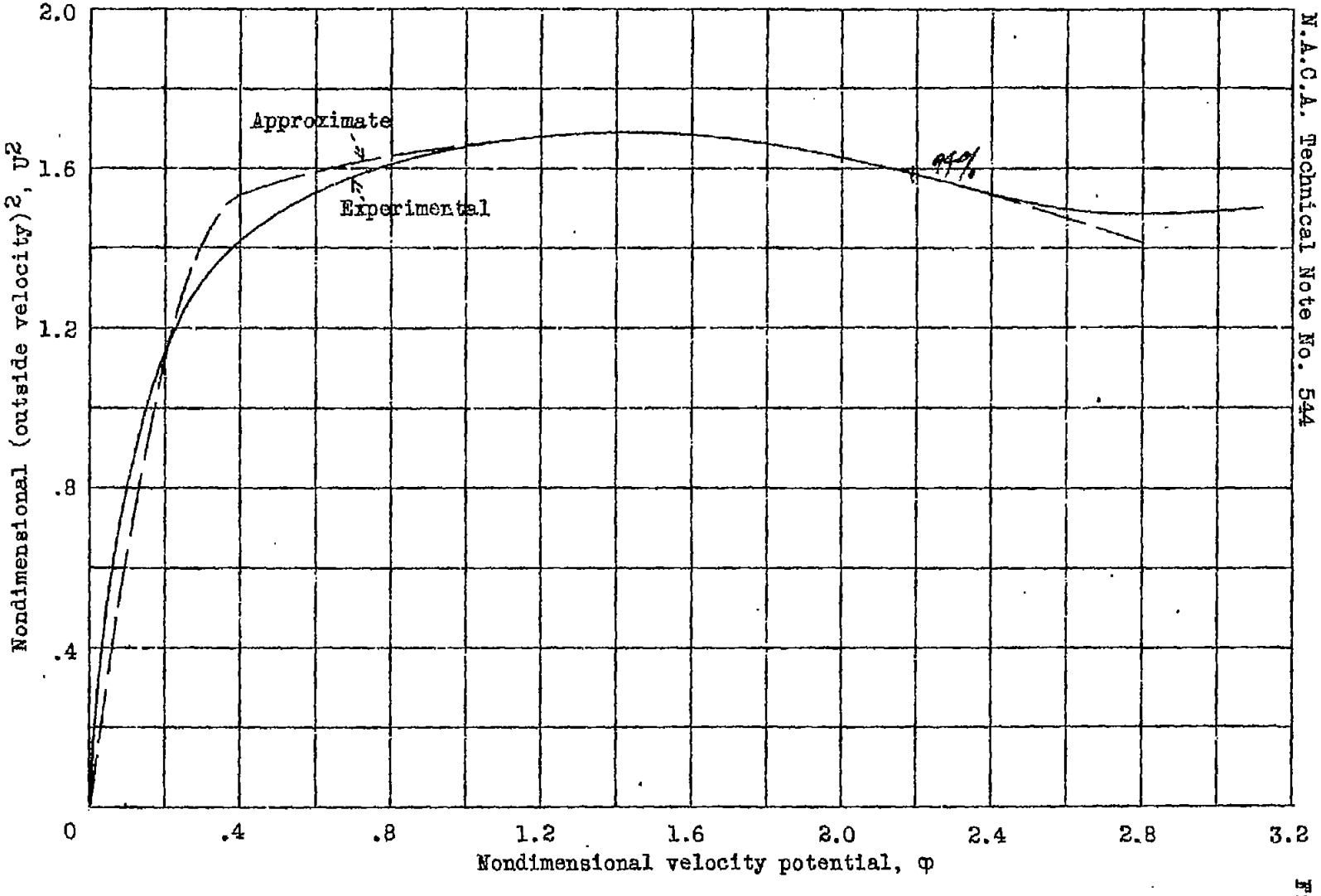

Figure 2.- Experimental and approximate U^2, φ curves.

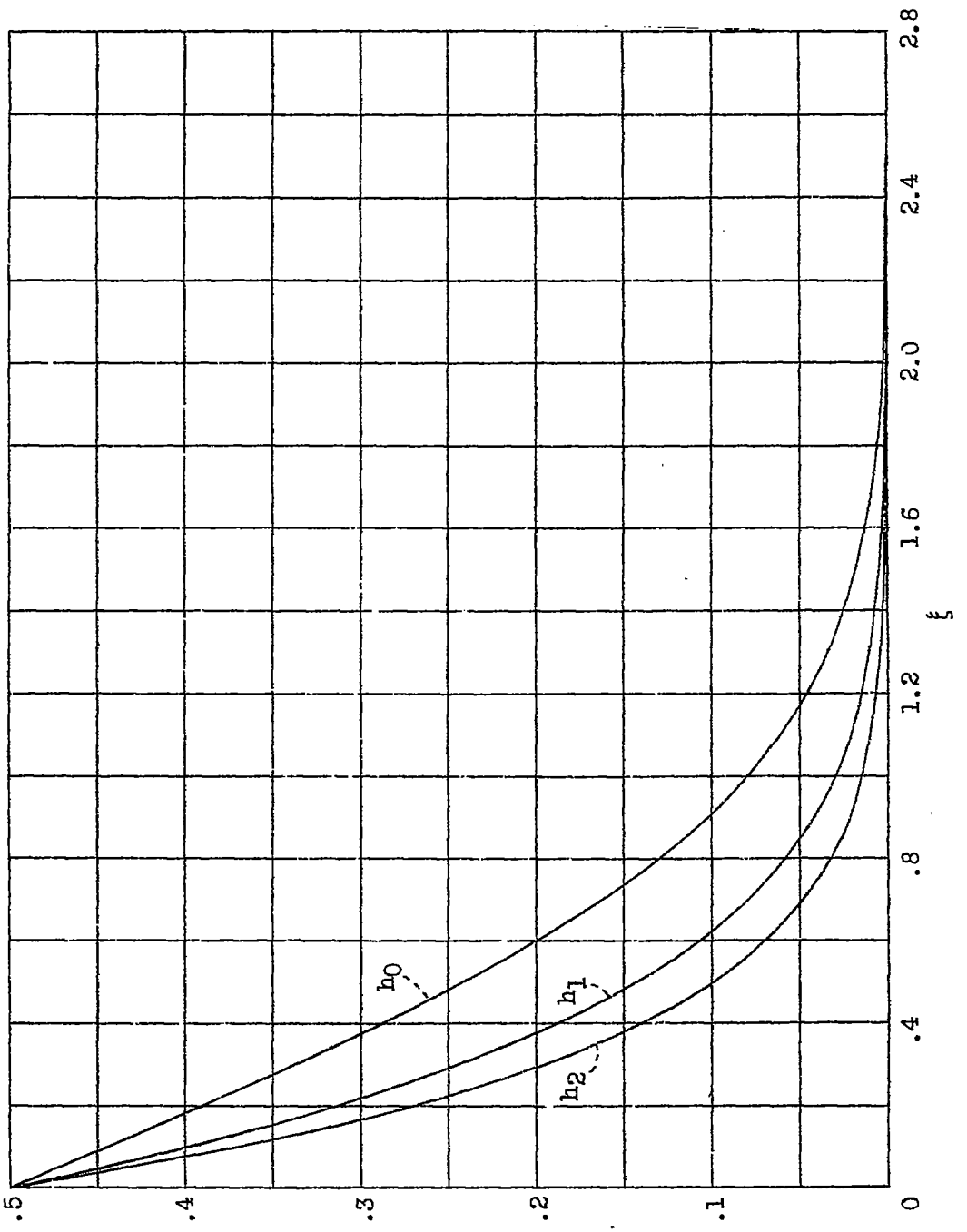

Figure 3.- The functions $h_0(\xi)$, $h_1(\xi)$, $h_2(\xi)$.

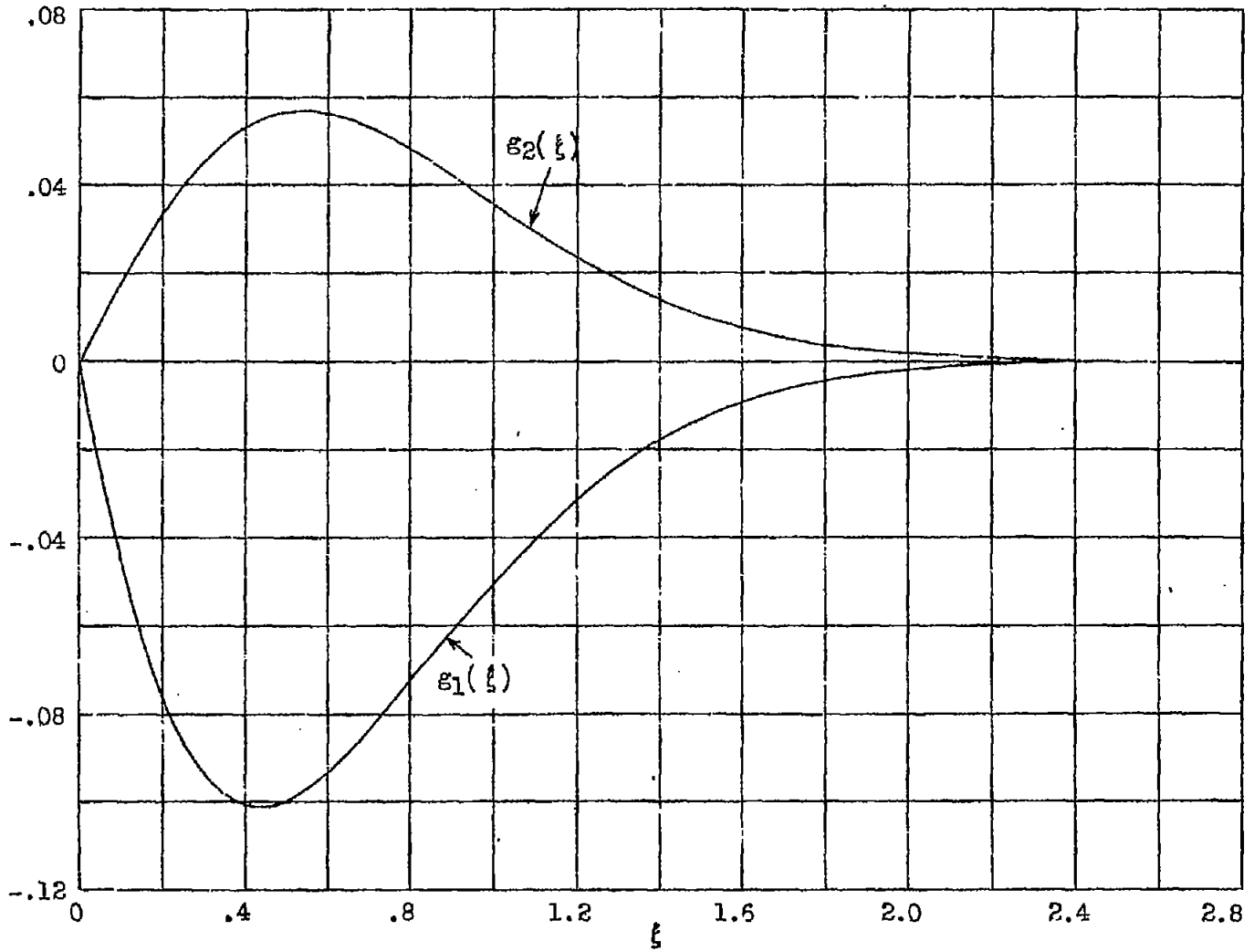

Figure 4.- The functions $g_1(\xi)$ and $g_2(\xi)$.

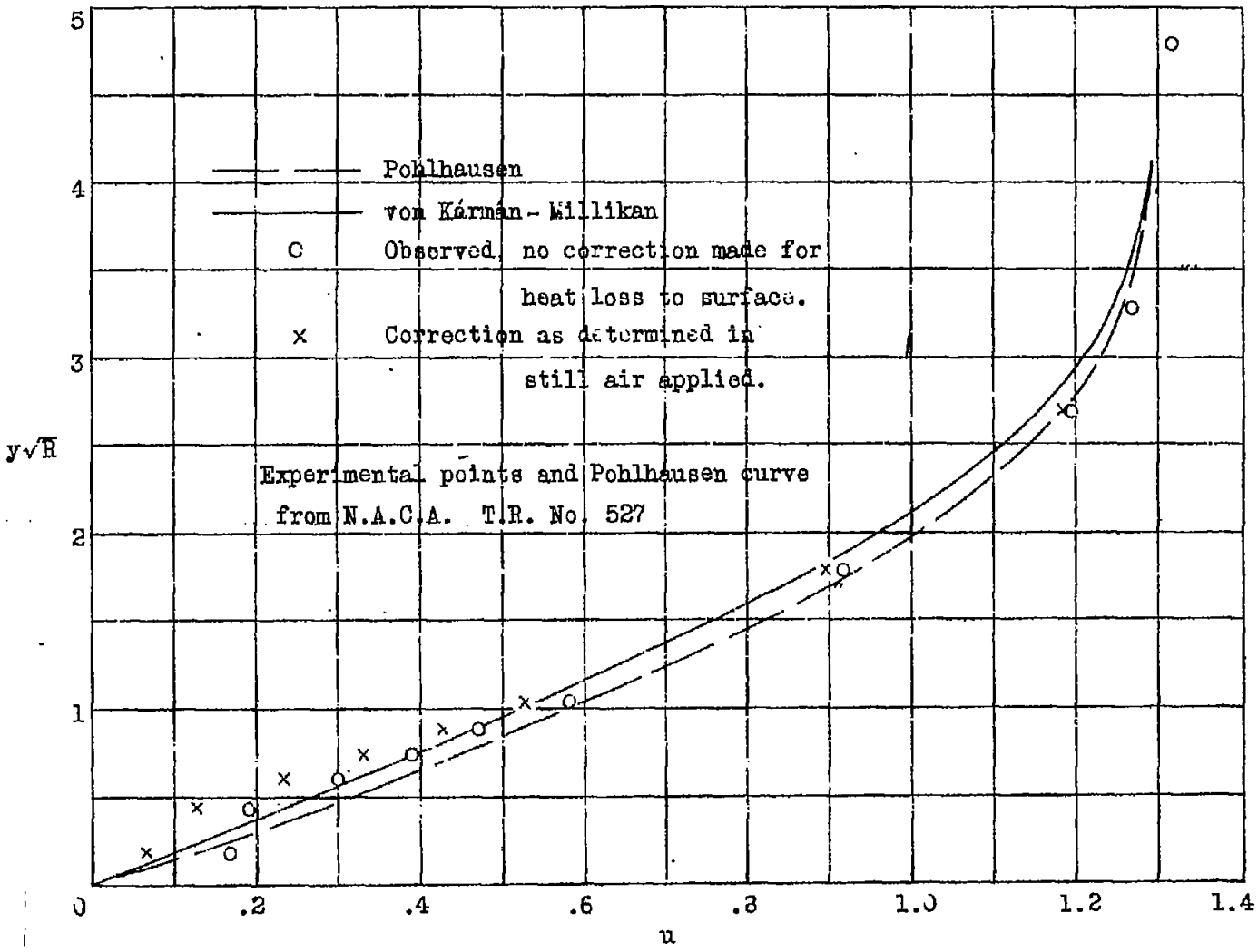

Figure 5.- Boundary-layer velocity distribution at s = 1.097.

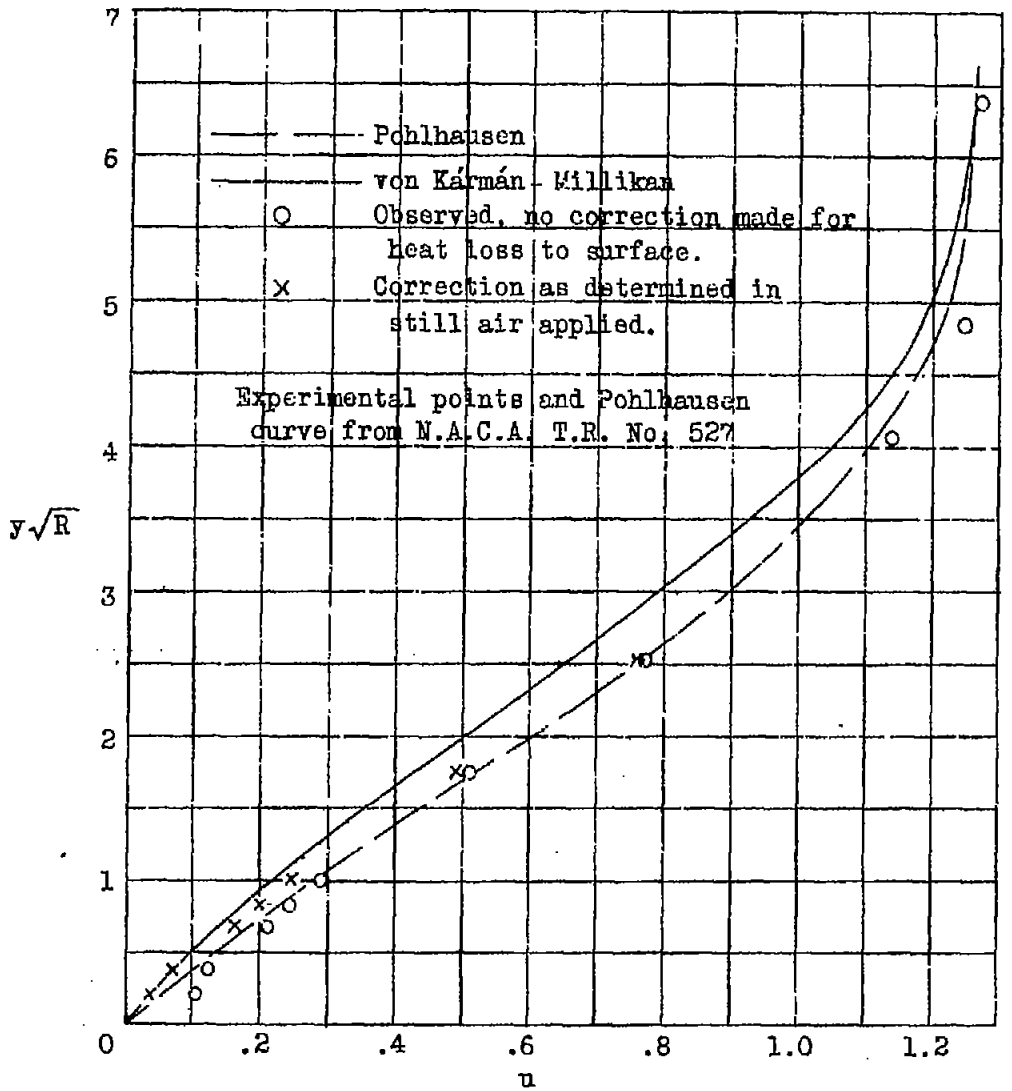

Figure 6.- Boundary-layer velocity distribution at s = 1.832.

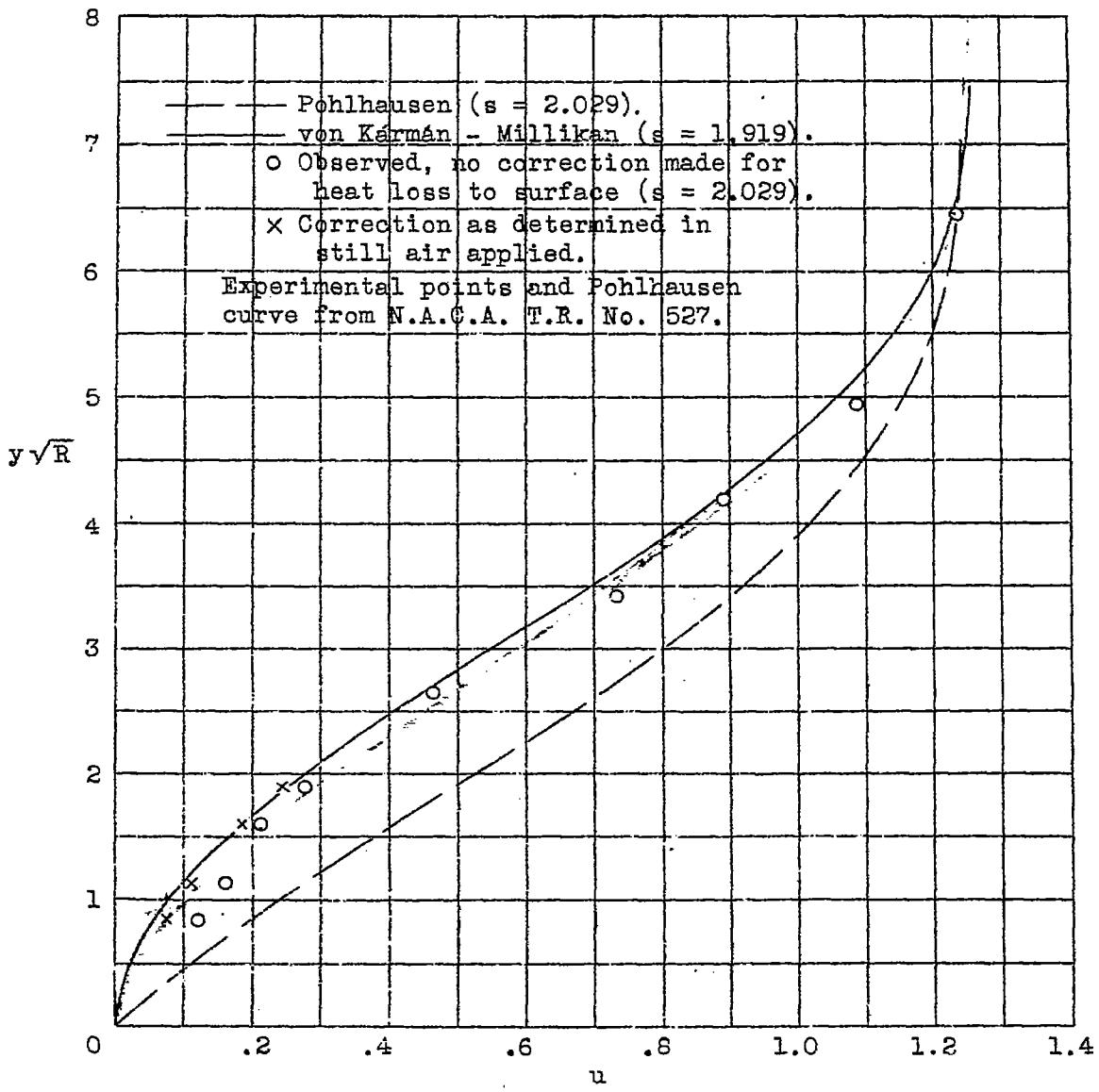

Figure 7.- Boundary-layer velocity distribution near separation point.

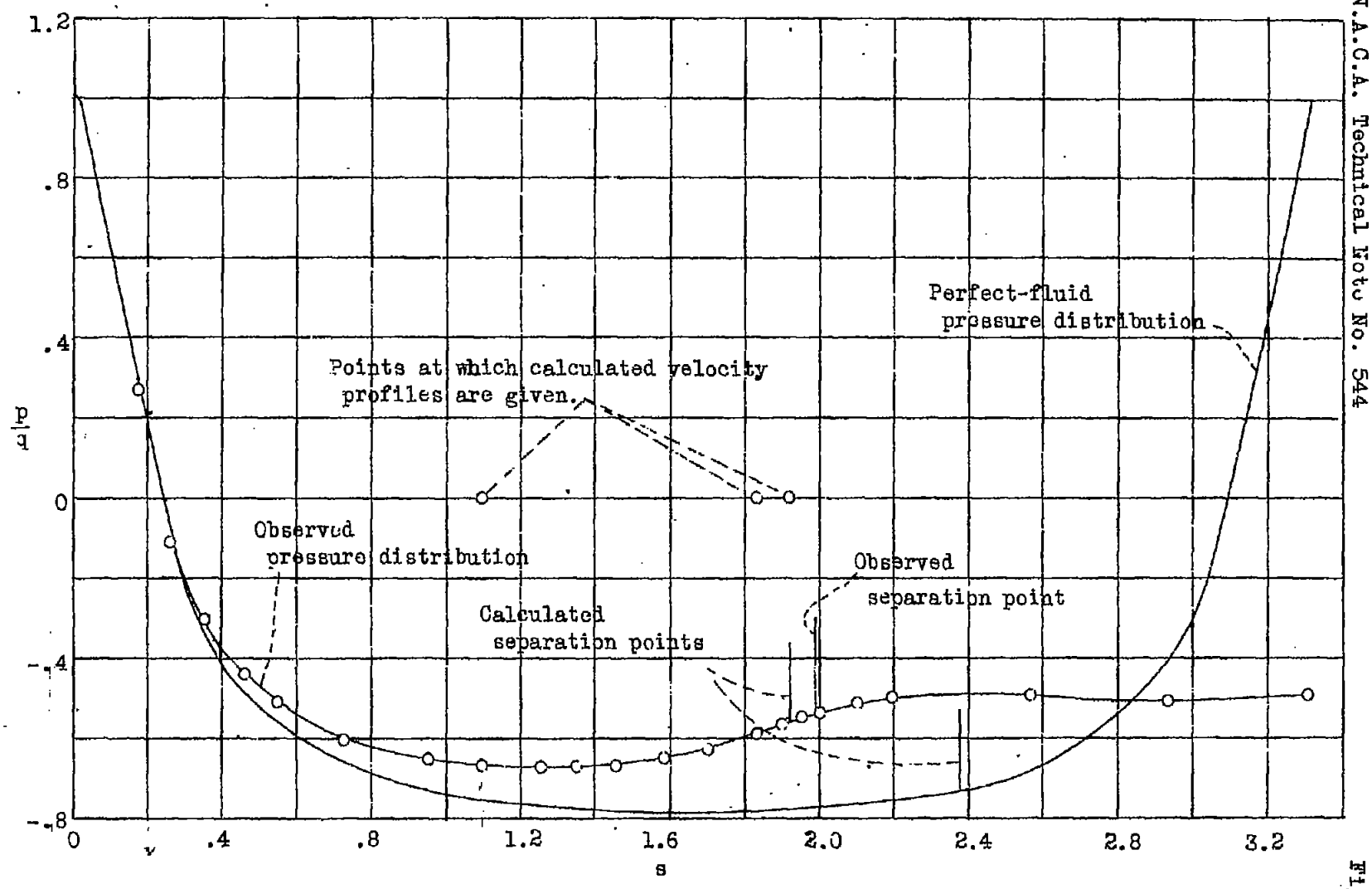

Figure 8.- Comparison of observed and calculated separation points.

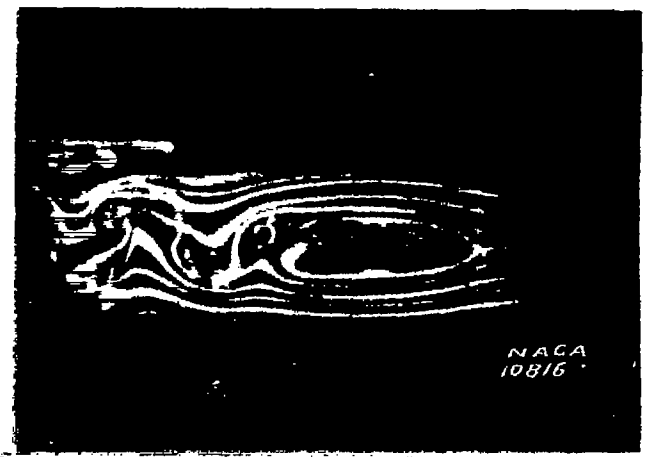

Figure 9.- Smoke-flow photograph of the flow about an elliptic cylinder.